

Hidden quantum correlations in the ground states of quasiclassical spin systems

Levente Rózsa,^{1,2} Dennis Wuhler,³ Sebastián A. Díaz,³ Ulrich Nowak,³ and Wolfgang Belzig³

¹*Department of Theoretical Solid State Physics, HUN-REN Wigner Research Centre for Physics, H-1525 Budapest, Hungary*

²*Department of Theoretical Physics, Budapest University of Technology and Economics, H-1111 Budapest, Hungary*

³*Department of Physics, University of Konstanz, 78457 Konstanz, Germany*

(Dated: November 14, 2024)

Frustrated spin models may lead to the formation of both classical non-collinear spin structures and unique quantum phases including highly entangled quantum spin liquids. Here, we study the entanglement and spatial quantum correlations in linear spin-wave theory around a classical spin-spiral ground state. We find that the entanglement between pairs of sites is short-ranged, and is completely absent in certain cases. In contrast, the entanglement hidden in multi-site clusters is peaked close to phase transitions and shows an asymptotic behavior modulated by the period of the magnetic structure. These findings motivate further exploring the connection in the entanglement properties of fully quantum and of quasiclassical spin models.

Strongly correlated quantum systems often give rise to exotic phases. The study of these phases has long been a strong driving force behind the development of analytical and numerical methods for treating correlated systems [1–3], as well as for the design of experiments and quantum simulations for their observation [4]. These phases are typically characterized by strong quantum entanglement, which has been demonstrated to show a scaling behavior at quantum phase transitions [5]. Due to their entangled ground state, strongly correlated quantum systems have been put forward as a robust quantum computing platform [6–8].

Spin models strongly coupled by exchange interactions provide a fertile ground for studying quantum correlations. Finding the ground state of such models is a daunting task, even for systems having a simple classical analogue such as the two-sublattice antiferromagnetic Heisenberg model. Exact solutions to this problem are available in one dimension for spin $S = 1/2$ for certain parameter ranges [9–11]. Although the ground state of an antiferromagnetic chain can rarely be constructed for higher spins, it has been proven that its excitation gap vanishes for infinite chains for half-integer spin [12], while for integer spin the system is conjectured to remain gapped [13, 14]. Numerical methods such as density-matrix renormalization group [1, 2] are especially well suited for one-dimensional systems. Antiferromagnetic interactions also give rise to strongly correlated magnetic phases in higher dimensions, for example quantum spin liquids characterized by a high degree of entanglement [15–17]. However, two- and three-dimensional systems are difficult to treat numerically in the fully quantum case, especially their correlations over long distances that require large system sizes.

Magnons or spin waves describe the excitations of magnetically ordered systems. In contrast to the strongly correlated phases, they may be calculated by an expansion starting from a non-fluctuating classical spin configuration, obtained in the $S \rightarrow \infty$ limit of the quantum model. Nevertheless, magnons follow bosonic statistics, and as such may be utilized in quantum information and communication based on continuous variables [18–20]. The

entanglement between magnons in single-mode ferromagnets or two-mode antiferromagnets and their correlations with cavity photons or phonons has been studied recently [21–26]. However, the limited number of modes considered in these previous works restricted the investigations to macroscopic quantum effects.

Non-collinear spin configurations such as spin spirals or skyrmions are present in a wide range of materials, and they possess intriguing topological and transport properties [27–29]. The spatial correlations in these textures are more complex than in ferromagnets or collinear antiferromagnets which can be described by a handful of modes. Non-collinear spin structures are stabilized by a competition between different interaction terms which often result in the formation of strongly correlated quantum phases as well [15]. The typical length scale of these structures ranges from a few nanometers to micrometers, but the investigation of their quantum properties [30, 31] has been hampered by the fact that available numerical methods only enable the study of the smallest sizes in this range even for two-dimensional systems [32–36]. While the properties of magnons in these systems has been widely studied in the classical limit [37], their quantum properties have been investigated much less, with the exception of magnon squeezing [38].

Here, we determine the entanglement between sites in non-collinear magnetic ground states based on quasiclassical spin-wave theory, illustrated on the example of spin spiral states. Going beyond macroscopic quantum effects, we consider all magnon modes in the system to study how the non-collinear structure modulates the entanglement on the atomic level. We demonstrate that the entanglement between pairs of sites is short-ranged and completely vanishes in certain parameter regimes, but find enhanced entanglement hidden in multi-site clusters close to phase transitions and at long distances. Finally, we discuss the analogy between the $S \rightarrow \infty$ quasiclassical and the $S = 1/2$ ultraquantum limit.

The entanglement in non-collinear spin structures in the linear spin-wave approximation can be calculated in the following steps. First, we determine the spin di-

rections $\mathbf{S}_i^{(0)}$ at each lattice site in the classical ground state based on the quantum model containing spin operators $\hat{\mathbf{S}}_i$. The classical ground state corresponds to the quantum state $|0\rangle_{\text{spin}} = \prod_i |S_i\rangle$, a product of maximally polarized eigenstates along the direction of $\mathbf{S}_i^{(0)}$, $\hat{\mathbf{S}}_i |S_i\rangle = S |S_i\rangle$. Second, we determine the low-energy excitations around this classical ground state within linear spin-wave theory by introducing bosonic creation and annihilation operators \hat{a}_i and \hat{a}_i^\dagger via the Holstein–Primakoff transformation [39]. This corresponds to approximating $|0\rangle_{\text{spin}}$ by a product of the ground states of harmonic oscillators, $|0\rangle_{\text{osc}} = \prod_i |0_i\rangle$ with $\hat{a}_i |0_i\rangle = 0$. Being product states, both $|0\rangle_{\text{spin}}$ and $|0\rangle_{\text{osc}}$ are completely uncorrelated between the different lattice sites. However, typically $|0\rangle_{\text{spin}}$ and $|0\rangle_{\text{osc}}$ do not correspond to the ground state or even any eigenstate of the Hamiltonian. Finding the fully quantum ground state in a space of dimension $(2S+1)^N$, where N is the number of lattice sites, is numerically a very challenging problem. Instead, we find the ground state of the linear spin-wave Hamiltonian, which is equivalent to finding the eigenvalues and eigenvectors of a matrix of size $2N \times 2N$, and introducing new annihilation operators $\hat{\alpha}_k$ as linear combinations of the \hat{a}_i and \hat{a}_i^\dagger . The so-called squeezed ground state, characterized by $\hat{\alpha}_k |\text{GS}\rangle = 0$, is an eigenstate of the spin-wave Hamiltonian, and has a lower energy than $|0\rangle_{\text{osc}}$. Third, we calculate the covariance matrix γ^a of the operators \hat{a}_i and \hat{a}_i^\dagger in the ground state $|\text{GS}\rangle$. Fourth, we select a subsystem in real space, separate it into two parts, and calculate the correlation between the parts. For this we use the relative information based on the von Neumann entropy $S_{V,\text{rel}}$, which contains both classical and quantum correlations, and the logarithmic negativity $E_{\mathcal{N}}$ [40], which measures exclusively quantum correlations for the bipartitions studied here [41]. Mathematical details of this procedure are given in the Supplemental Material [42].

As an example, we consider the Heisenberg model on the triangular lattice,

$$\hat{\mathcal{H}} = \frac{1}{2} \sum_{\langle i,j \rangle_d} J_d \hat{\mathbf{S}}_i \cdot \hat{\mathbf{S}}_j, \quad (1)$$

where $\hat{\mathbf{S}}_i$ is the spin operator at lattice site i , J_d are the exchange interactions, and $d = 1$ and 2 denote nearest- and next-nearest-neighbors, respectively. The classical ground state corresponds to the spins being oriented along the $\mathbf{S}_i = \cos(\mathbf{q}_0 \mathbf{R}_i) \mathbf{e}_1 + \sin(\mathbf{q}_0 \mathbf{R}_i) \mathbf{e}_2$ direction, where \mathbf{R}_i is the position of site i , \mathbf{e}_1 and \mathbf{e}_2 are orthonormal vectors, and the wave vector \mathbf{q}_0 is chosen such that it minimizes the Fourier transform of the Heisenberg interactions $J_{\mathbf{q}}$. If J_1 or J_2 is positive or antiferromagnetic, the energy is minimized for a finite wave vector \mathbf{q}_0 , and the spins form a harmonic spin spiral in the plane spanned by \mathbf{e}_1 and \mathbf{e}_2 . Further calculation details are given in the Supplemental Material [42].

The calculated ground state and the correlation measures are illustrated in Fig. 1 for $J_2 = -J_1 > 0$. The rel-

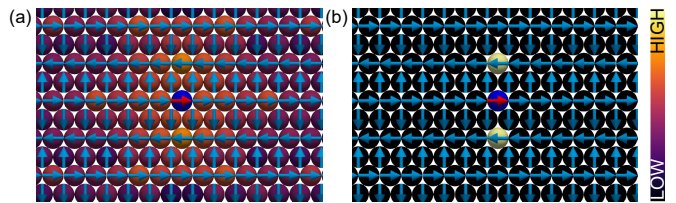


FIG. 1. Spatial distribution of magnonic pair correlation measures in spin spirals. (a) Pairwise relative von Neumann information $S_{V,\text{rel,pw}}$ and (b) pairwise logarithmic negativity $E_{\mathcal{N},\text{pw}}$ between the center site (red arrow in blue sphere) and the other sites. The color of the spheres shows the magnitude of the correlations with that site, with the color scale being logarithmic. Arrows illustrate the classical spin spiral ground state. The exchange interactions take the value $J_2 = -J_1 > 0$, resulting in a spin spiral with 4 atoms period along the y direction, $q_0^y = 2\pi / (2\sqrt{3}a)$. The Brillouin zone integration was performed on an $N = 513 \times 513$ grid. In stark contrast to the classical correlations in panel (a), the quantum correlations in panel (b) are anisotropic and short-ranged.

ative information calculated from the von Neumann entropy $S_{V,\text{rel,pw}}$ for pairs of sites in Fig. 1(a) decays as the distance between the sites increases, but remains finite up to arbitrarily large distances. It can also be observed that the relative information is spatially modulated by the spin spiral structure, resulting in an oscillatory decay not only along the spiral modulation direction y , but along the perpendicular direction x as well. In contrast, the logarithmic negativity calculated for pairs of sites is only finite for next-nearest-neighbors along the y direction, while it is equal to zero for all other neighbors. The surprisingly short range of quantum correlations compared to classical correlations has also been observed for one-dimensional quantum spin chains in Ref. [5], indicating a qualitative similarity between the entanglement calculated in the ground state of the spin Hamiltonian there and in the spin-wave Hamiltonian considered here.

The entanglement is analyzed in an extended parameter space in Fig. 2. Here we set $J_2 > 0$ and varied J_1 from positive to negative values. As illustrated by the blue curve, four different phases can be observed in the system, the boundaries between which may be determined by minimizing $J_{\mathbf{q}}$ with respect to the wave vector. For only nearest-neighbour antiferromagnetic interactions, the ground state is the three-sublattice Néel state with $q_0^x = 4\pi / (3a)$, $q_0^y = 0$. This transforms into a row-wise antiferromagnetic state at $J_2/J_1 = 1/8$ with $q_0^x = 0$, $q_0^y = 2\pi / (\sqrt{3}a)$. At the transition between the two type of antiferromagnetic states, these two states are degenerate with all other spin spirals with modulation vectors \mathbf{q}_0 along the boundary of the atomic Brillouin zone. This extensive ground-state degeneracy is required for classical spin liquids [43]. For $J_2/J_1 \geq 1$, the wave vector of the spiral starts to decrease while keeping its orientation along the next-nearest-neighbor direction in real space. The period of the spiral diverges at $J_2/J_1 = -1/3$, and the system becomes ferromagnetically aligned.

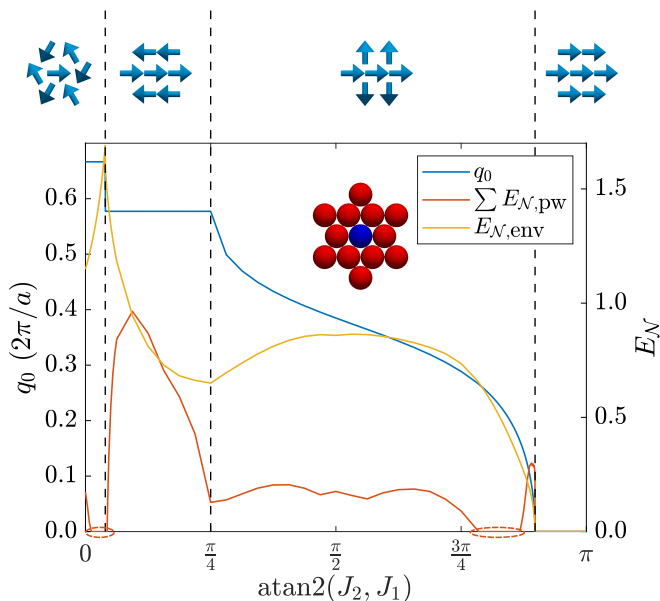


FIG. 2. Phase diagram and logarithmic negativity. Ordering wave vector of the spiral q_0 , pairwise logarithmic negativity $\sum E_{N,pw}$ summed up over all sites, and logarithmic negativity $E_{N,env}$ with the environment as a function of the ratio of nearest-neighbor and next-nearest-neighbor exchange couplings. Sketches at the top illustrate from left to right the Néel antiferromagnetic state, the row-wise antiferromagnetic state, the spin-spiral state, and the ferromagnetic state. The center site (blue) and the environment containing all nearest- and next-nearest-neighbour sites (red) used as a bipartition for calculating $E_{N,env}$ is also sketched. Dashed orange ellipses highlight the regions where $\sum E_{N,pw}$ vanishes but $E_{N,env}$ remains finite. The Brillouin zone integration was performed on an $N = 513 \times 513$ grid. Multiple-site clusters, rather than pairs of sites, are required to reveal the hidden quantum entanglement.

Calculating the logarithmic negativity between pairs of sites, and summing it up over all relative positions by taking advantage of its finite range, results in the orange curve in Fig. 2. The pairwise logarithmic negativity vanishes in the isotropic ferromagnetic state, since this is completely uncorrelated both in the spin-wave description and in the original spin Hamiltonian. The entanglement between pairs starts to increase in the spin-spiral phase, before abruptly vanishing in the range $2.47 \leq \text{atan2}(J_2, J_1) \leq 2.72$. In this regime, the range of the pairwise logarithmic negativity is 0, and no pairwise quantum correlations can be observed. The logarithmic negativity again increases for shorter spin-spiral periods, and assumes even higher values in the row-wise antiferromagnetic phase. However, it again vanishes in the range $0.037 \leq \text{atan2}(J_2, J_1) \leq 0.136$, including the phase transition point between the two antiferromagnetic phases.

We also considered a 13-atom cluster sketched in Fig. 2, and calculated the logarithmic negativity over the bipartition into the central atom and all other atoms, as shown by the yellow curve. The logarithmic negativity calcu-

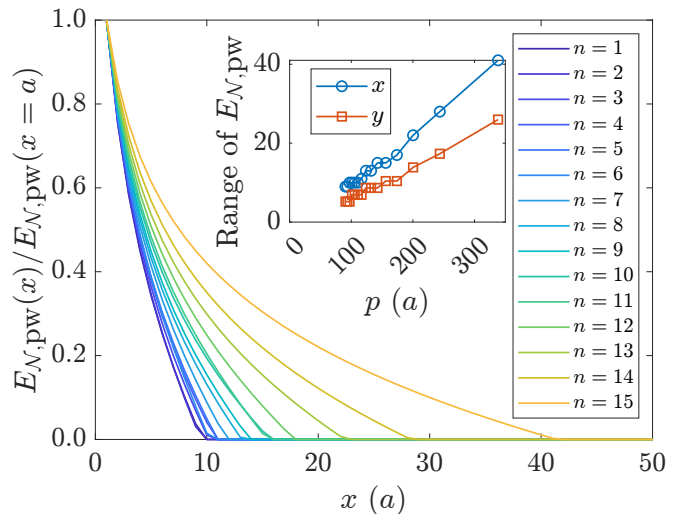


FIG. 3. Pairwise logarithmic negativity close to the spin spiral-ferromagnetic transition. The pairwise logarithmic negativity $E_{N,pw}$ is calculated for neighbours along the x direction, and normalized to the nearest-neighbour value. The interaction parameters are $\text{atan2}(J_2, J_1) = 919\pi/2^{10} + n\pi/2^{17}$. Inset shows the range of $E_{N,pw}$ as a function of the spin-spiral period p . The Brillouin zone integration was performed on an $N = 1026 \times 1026$ grid. The range of quantum correlations in spin spirals increases almost linearly with the spiral period.

lated with this environment only vanishes in the uncorrelated ferromagnetic state, but it becomes finite in the regimes inside the correlated spin spiral and antiferromagnetic phases where no pairwise logarithmic negativity was found. This means that the entanglement in these parameter ranges cannot be extracted when looking at only two lattice sites, instead it is hidden in clusters consisting of multiple sites. Well-known examples of analogous multipartite entanglement for three spin-1/2 particles include the GHZ state [44] and the W state [45]. Particularly interesting is the phase transition between the Néel and the row-wise antiferromagnetic states, where the pairwise logarithmic negativity vanishes but the value calculated for the larger cluster reaches a maximum when approaching from either side. The full Heisenberg spin Hamiltonian has long been considered as a highly entangled quantum-spin-liquid candidate in the vicinity of this classical phase transition [17], while in quasiclassical spin-wave theory we find an enhanced but exclusively multipartite entanglement.

The logarithmic negativity between pairs of sites is further investigated close to the transition from the spin spiral to the ferromagnetic state in Fig. 3. The range of this type of correlation increases with the period of the spiral approximately linearly, as shown in the inset. However, it remains much shorter than the period. This type of quantum correlation extends up to larger distances perpendicular to the spiral modulation direction (x) than along the modulation direction (y). Note that the amplitude of the logarithmic negativity decreases as the phase

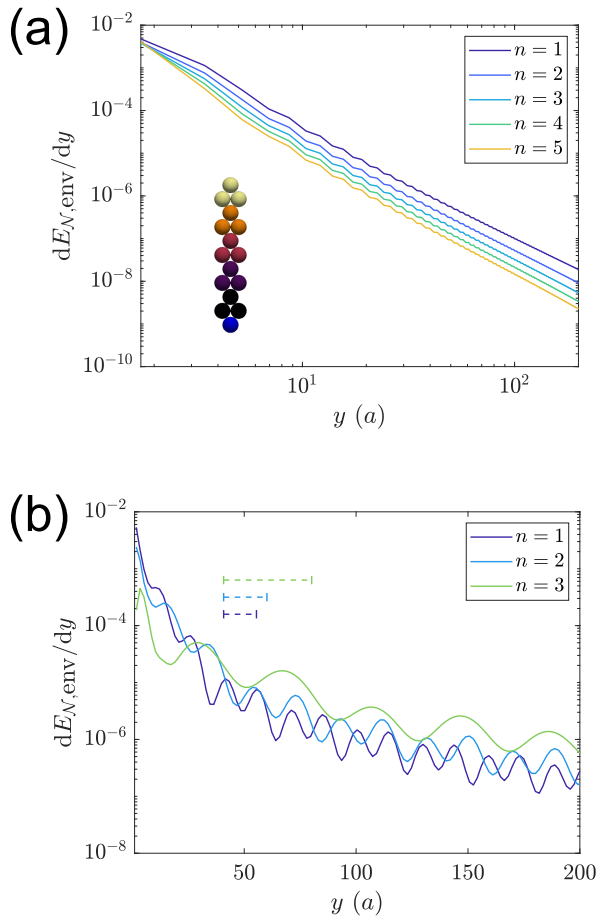


FIG. 4. Derivative of the logarithmic negativity with the environment along the modulation direction (a) close to the transition from the row-wise antiferromagnetic state to the Néel antiferromagnetic state ($\text{atan2}(J_2, J_1) = 5\pi/2^7 + n\pi/2^8$) and (b) close to the transition from the spin-spiral state to the ferromagnetic state ($\text{atan2}(J_2, J_1) = 1829\pi/2^{11} + n\pi/2^9$). The logarithmic negativity was calculated for the bipartition on the lowest site (blue) and the environment (yellow to purple atoms). In each step, the environment was increased by three atoms denoted by the same color. $dE_{\mathcal{N},\text{env}}/dy$ is the logarithmic negativity differentiated with respect to the size of the environment. Dashed lines in panel (b) illustrate the spin-spiral period p for the given parameters. The Brillouin zone integration was performed on an $N = 1026 \times 1026$ grid. The power-law decay of $dE_{\mathcal{N},\text{env}}/dy$ in the vicinity of both transitions is consistent with a gapless excitation spectrum. The Goldstone mode associated with the free choice of the rotational plane of the spiral causes the spatial modulation.

transition is approached (see Fig. 2), but Fig. 3 shows the curves normalized to the nearest-neighbor value for better visibility.

The logarithmic negativity between pairs of sites is not suitable for studying the asymptotic behaviour of quantum correlations, since it has a short range and com-

pletely vanishes in certain parameter regimes. As an alternative measure, we considered the logarithmic negativity between a site and its increasingly larger environment along a certain direction, illustrated by the sketch in Fig. 4(a). The $E_{\mathcal{N},\text{env}}$ calculated this way monotonically increases with the size of the environment. We also calculated $dE_{\mathcal{N},\text{env}}/dy$, i.e., the increase in $E_{\mathcal{N},\text{env}}$ when three additional atoms are added to the cluster divided by $\Delta y = \sqrt{3}a$, and found that it converges to zero. Similarly to the decaying function $S_{V,\text{rel,pw}}$, $dE_{\mathcal{N},\text{env}}/dy$ may be considered as a correlation function, describing by how much the quantum correlations between a site and its environment increase by adding further sites to the cluster at a given distance. We considered a three-atom-wide environment because close to the transition between the two antiferromagnetic states, the logarithmic negativity does not only vanish for all pairs of sites but between sites and their one-atom-wide extensions as well. Approaching this phase transition from the row-wise antiferromagnetic state, it can be seen from the linear behavior on the log-log scale in Fig. 4(a) that $dE_{\mathcal{N},\text{env}}/dy$ may be well approximated by a power function. This behavior is expected for a system with an ungapped excitation spectrum, connected to the translation of the spiral on the lattice; see the Supplemental Material [42]. The exponent of the function approaches zero closer to the transition point; see the Supplemental Material [42] for the fitting parameters. At the phase transition, the extensive ground-state degeneracy results in nodal lines in the magnon spectrum where the frequency vanishes, and a divergence of the correlations.

A similar power-law decay of $dE_{\mathcal{N},\text{env}}/dy$ is observed close to the transition from the spin spiral to the ferromagnetic state in Fig. 4(b). The spatial modulation of the correlation function is also apparent in this case, and the highest Fourier component of this modulation approximately corresponds to the period of the spin spiral along the considered y direction, as illustrated by the dashed segments. This modulation is caused by the zero mode connected to the free choice of the rotational plane of the spiral, see the Supplemental Material [42]. The modulation is not apparent in Fig. 4(a) because the period of the modulation in the row-wise antiferromagnetic state coincides with the next-nearest-neighbor distance along y , which is precisely the step size with which the environment is increased.

In summary, we investigated correlations in non-collinear magnetic ground states based on quasiclassical linear spin-wave theory. We used the relative information calculated from the von Neumann entropy to describe both classical and quantum correlations, and the logarithmic negativity for calculating exclusively quantum correlations or entanglement. In a nearest- and next-nearest-neighbour Heisenberg model on the triangular lattice, we found that the entanglement between pairs of sites has short range, and it vanishes completely around the transition point between the row-wise antiferromagnetic and the Néel antiferromagnetic phases, as

well as in a regime inside the spin-spiral phase. In these regions, the entanglement is hidden in multisite clusters. We calculated the asymptotic behaviour of the entanglement by studying clusters of increasing size, and found that the derivative of the logarithmic negativity with respect to the cluster size follows a power-law decay modulated by the spin-spiral structure, with the exponent approaching zero at the phase transitions where magnon correlations diverge. The short-range nature of the entanglement and its unusual behavior close to the classical phase transition between the row-wise and Néel antiferromagnetic states correlates with previous observations in fully quantum spin models. Established experimental methods and first-principles calculations may be utilized to design the magnetic interactions for engineering non-collinear structures [28], enabling the exploration of an extended parameter space in real materials. State-of-the-art imaging techniques already enable resolving the magnetic structure on the atomic scale [46–48], and might be developed further towards measuring spin fluctuations. The low computational complexity of spin-wave theory should facilitate the exploration of entanglement prop-

erties at long distances in two- or three-dimensions, the study of the scaling law of entanglement in these models, and the investigation of utilizing quasiclassical systems for quantum information processing.

ACKNOWLEDGMENTS

This work was financially supported by the Deutsche Forschungsgemeinschaft (DFG, German Research Foundation) via the Collaborative Research Center SFB 1432 (project no. 425217212), by the National Research, Development, and Innovation Office (NRDI) of Hungary under Project Nos. K131938 and FK142601, by the Ministry of Culture and Innovation and the National Research, Development and Innovation Office within the Quantum Information National Laboratory of Hungary (Grant No. 2022-2.1.1-NL-2022-00004), and by the Hungarian Academy of Sciences via a János Bolyai Research Grant (Grant No. BO/00178/23/11).

-
- [1] S. R. White, *Phys. Rev. Lett.* **69**, 2863 (1992).
 - [2] S. R. White, *Phys. Rev. B* **48**, 10345 (1993).
 - [3] R. Orús, *Nature Reviews Physics* **1**, 538–550 (2019).
 - [4] I. M. Georgescu, S. Ashhab, and F. Nori, *Rev. Mod. Phys.* **86**, 153 (2014).
 - [5] A. Osterloh, L. Amico, G. Falci, and R. Fazio, *Nature* **416**, 608–610 (2002).
 - [6] G. K. Brennen and A. Miyake, *Phys. Rev. Lett.* **101**, 010502 (2008).
 - [7] X. Chen, B. Zeng, Z.-C. Gu, B. Yoshida, and I. L. Chuang, *Phys. Rev. Lett.* **102**, 220501 (2009).
 - [8] T.-C. Wei, I. Affleck, and R. Raussendorf, *Phys. Rev. Lett.* **106**, 070501 (2011).
 - [9] H. Bethe, *Zeitschrift für Physik* **71**, 205–226 (1931).
 - [10] E. Lieb, T. Schultz, and D. Mattis, *Annals of Physics* **16**, 407–466 (1961).
 - [11] C. K. Majumdar and D. K. Ghosh, *Journal of Mathematical Physics* **10**, 1388–1398 (1969).
 - [12] I. Affleck and E. H. Lieb, *Letters in Mathematical Physics* **12**, 57–69 (1986).
 - [13] F. D. M. Haldane, *Phys. Rev. Lett.* **50**, 1153 (1983).
 - [14] F. Haldane, *Physics Letters A* **93**, 464–468 (1983).
 - [15] L. Balents, *Nature* **464**, 199–208 (2010).
 - [16] L. Savary and L. Balents, *Reports on Progress in Physics* **80**, 016502 (2016).
 - [17] Z. Zhu and S. R. White, *Phys. Rev. B* **92**, 041105 (2015).
 - [18] S. L. Braunstein and P. van Loock, *Rev. Mod. Phys.* **77**, 513 (2005).
 - [19] J. Eisert and M. B. Plenio, *International Journal of Quantum Information* **01**, 479–506 (2003).
 - [20] G. Adesso and F. Illuminati, *Journal of Physics A: Mathematical and Theoretical* **40**, 7821–7880 (2007).
 - [21] A. Kamra, E. Thingstad, G. Rastelli, R. A. Duine, A. Brataas, W. Belzig, and A. Sudbø, *Phys. Rev. B* **100**, 174407 (2019).
 - [22] Z. Zhang, M. O. Scully, and G. S. Agarwal, *Phys. Rev. Res.* **1**, 023021 (2019).
 - [23] J. Li and S.-Y. Zhu, *New Journal of Physics* **21**, 085001 (2019).
 - [24] H. Y. Yuan, S. Zheng, Z. Ficek, Q. Y. He, and M.-H. Yung, *Phys. Rev. B* **101**, 014419 (2020).
 - [25] H. Y. Yuan, A. Kamra, D. M. F. Hartmann, and R. A. Duine, *Phys. Rev. Appl.* **16**, 024047 (2021).
 - [26] H. Yuan, Y. Cao, A. Kamra, R. A. Duine, and P. Yan, *Physics Reports* **965**, 1 (2022).
 - [27] K. v. Bergmann, A. Kubetzka, O. Pietzsch, and R. Wiesendanger, *Journal of Physics: Condensed Matter* **26**, 394002 (2014).
 - [28] C. Back, V. Cros, H. Ebert, K. Everschor-Sitte, A. Fert, M. Garst, T. Ma, S. Mankovsky, T. L. Monchesky, M. Mostovoy, N. Nagaosa, S. S. P. Parkin, C. Pfleiderer, N. Reyren, A. Rosch, Y. Taguchi, Y. Tokura, K. von Bergmann, and J. Zang, *Journal of Physics D: Applied Physics* **53**, 363001 (2020).
 - [29] B. Göbel, I. Mertig, and O. A. Tretiakov, *Physics Reports Beyond skyrmions: Review and perspectives of alternative magnetic quasiparticles*, **895**, 1 (2021).
 - [30] C. Psaroudaki and C. Panagopoulos, *Phys. Rev. Lett.* **127**, 067201 (2021).
 - [31] A. Haller, S. A. Díaz, W. Belzig, and T. L. Schmidt, *Quantum magnetic skyrmion operator* (2024).
 - [32] V. Lohani, C. Hickey, J. Masell, and A. Rosch, *Phys. Rev. X* **9**, 041063 (2019).
 - [33] O. M. Sotnikov, V. V. Mazurenko, J. Colbois, F. Mila, M. I. Katsnelson, and E. A. Stepanov, *Phys. Rev. B* **103**, L060404 (2021).
 - [34] P. Siegl, E. Y. Vedmedenko, M. Stier, M. Thorwart, and T. Posske, *Phys. Rev. Res.* **4**, 023111 (2022).
 - [35] A. Haller, S. Groenendijk, A. Habibi, A. Michels, and T. L. Schmidt, *Phys. Rev. Res.* **4**, 043113 (2022).

- [36] A. Joshi, R. Peters, and T. Posske, *Phys. Rev. B* **110**, 104411 (2024).
- [37] M. Garst, J. Waizner, and D. Grundler, *Journal of Physics D: Applied Physics* **50**, 293002 (2017).
- [38] D. Wuhrer, L. Rózsa, U. Nowak, and W. Belzig, *Phys. Rev. Res.* **5**, 043124 (2023).
- [39] T. Holstein and H. Primakoff, *Phys. Rev.* **58**, 1098 (1940).
- [40] G. Vidal and R. F. Werner, *Phys. Rev. A* **65**, 032314 (2002).
- [41] R. Simon, *Phys. Rev. Lett.* **84**, 2726 (2000).
- [42] See Supplemental Material at [] containing the method of calculating the correlation measures, further details about the correlation matrix in spin spirals, and the fitting of the asymptotics of the correlation functions. It also contains Refs. [49–56].
- [43] H. Yan, O. Benton, R. Moessner, and A. H. Nevidomskyy, *Phys. Rev. B* **110**, L020402 (2024).
- [44] D. M. Greenberger, M. A. Horne, and A. Zeilinger, *Going Beyond Bell's Theorem* (2007).
- [45] W. Dür, G. Vidal, and J. I. Cirac, *Phys. Rev. A* **62**, 062314 (2000).
- [46] R. Wiesendanger, *Rev. Mod. Phys.* **81**, 1495 (2009).
- [47] A. Schlenhoff, i. c. v. c. v. Kovařík, S. Krause, and R. Wiesendanger, *Phys. Rev. Lett.* **123**, 087202 (2019).
- [48] T. Tanigaki, T. Akashi, T. Yoshida, K. Harada, K. Ishizuka, M. Ichimura, K. Mitsuishi, Y. Tomioka, X. Yu, D. Shindo, Y. Tokura, Y. Murakami, and H. Shinada, *Nature* **631**, 521–525 (2024).
- [49] L. D. Landau and E. M. Lifshitz, *Phys. Z. Sowjetunion* **8**, 153 (1935).
- [50] T. L. Gilbert, *IEEE Trans. Magn.* **40**, 3443 (2004).
- [51] A. Peres, *Phys. Rev. Lett.* **77**, 1413 (1996).
- [52] M. Horodecki, P. Horodecki, and R. Horodecki, *Physics Letters A* **223**, 1–8 (1996).
- [53] T. Moriya, *Phys. Rev.* **120**, 91 (1960).
- [54] I. Dzyaloshinsky, *Journal of Physics and Chemistry of Solids* **4**, 241 (1958).
- [55] H. J. Monkhorst and J. D. Pack, *Phys. Rev. B* **13**, 5188 (1976).
- [56] J. D. Pack and H. J. Monkhorst, *Phys. Rev. B* **16**, 1748 (1977).

Supplemental Material to Hidden quantum correlations in the ground states of quasiclassical spin systems

Levente Rózsa,^{1,2} Dennis Wuhler,³ Sebastián A. Díaz,³ Ulrich Nowak,³ and Wolfgang Belzig³

¹*Department of Theoretical Solid State Physics, HUN-REN Wigner Research Centre for Physics, H-1525 Budapest, Hungary*

²*Department of Theoretical Physics, Budapest University of Technology and Economics, H-1111 Budapest, Hungary*

³*Department of Physics, University of Konstanz, 78457 Konstanz, Germany*

(Dated: November 14, 2024)

Here we discuss the method of calculating the correlation measures, give further details about the correlation matrix in spin spirals, and provide the fitting parameters of the asymptotics of the correlation functions.

S.I. COVARIANCE MATRIX AND CORRELATION MEASURES IN GENERAL NON-COLLINEAR STRUCTURES

Here, we discuss the mathematical procedure for calculating the entanglement measures. The classical ground state $\mathbf{S}_i^{(0)}$ generally can only be determined numerically. For the spin spiral discussed in the main text, this simplifies to minimizing $J_{\mathbf{q}}$ in the Brillouin zone. In more complicated cases, the torque acting on the spins has to be minimized at each lattice site simultaneously, for example via the numerical solution of the Landau–Lifshitz–Gilbert equation [1, 2]. To calculate the spin waves, we introduce a right-handed orthonormal basis $\{\mathbf{e}_{i,1}, \mathbf{e}_{i,2}, \mathbf{e}_{i,3} = \mathbf{S}_i^{(0)}\}$ at each lattice site, and express the components of the spin operators in this basis $\hat{S}_{i,\alpha} = \hat{\mathbf{S}}_i \cdot \mathbf{e}_{i,\alpha}$ using the linearized Holstein–Primakoff transformation [3],

$$\hat{S}_{i,1} = \sqrt{\frac{S}{2}} (\hat{a}_i + \hat{a}_i^\dagger) = \sqrt{S} \hat{q}_i, \quad (\text{S.1})$$

$$\hat{S}_{i,2} = -i\sqrt{\frac{S}{2}} (\hat{a}_i - \hat{a}_i^\dagger) = \sqrt{S} \hat{p}_i, \quad (\text{S.2})$$

$$\hat{S}_{i,3} = S - \hat{a}_i^\dagger \hat{a}_i, \quad (\text{S.3})$$

where S is the spin quantum number, $[\hat{a}_i, \hat{a}_j^\dagger] = \delta_{ij}$ are bosonic creation and annihilation operators, and $[q_i, p_j] = i\delta_{ij}$ are conjugate generalized coordinates and momenta. Substituting this transformation into the Hamiltonian in Eq. (1) in the main text and keeping terms only up to second order in the bosonic operators yields

$$\hat{\mathcal{H}}_{\text{SW}} = E_0 + \frac{1}{2} \sum_{i,j}^N (\omega_{ij} \hat{a}_i^\dagger \hat{a}_j + \mu_{ij} \hat{a}_i \hat{a}_j + \text{h. c.}), \quad (\text{S.4})$$

where N is the number of sites, E_0 is the classical ground-state energy, and ω_{ij} and μ_{ij} are coefficients of the spin-wave Hamiltonian.

To find the ground state $|\text{GS}\rangle$ of $\hat{\mathcal{H}}_{\text{SW}}$, we look for bosonic operators $\hat{\alpha} = (\hat{\alpha}_1, \dots, \hat{\alpha}_N, \hat{\alpha}_1^\dagger, \dots, \hat{\alpha}_N^\dagger)$ as linear combinations of the original operators $\hat{\mathbf{a}} =$

$$(\hat{a}_1, \dots, \hat{a}_N, \hat{a}_1^\dagger, \dots, \hat{a}_N^\dagger),$$

$$\hat{\alpha} = \mathcal{U}^{-1} \hat{\mathbf{a}}, \quad (\text{S.5})$$

with the condition that they diagonalize the spin-wave Hamiltonian,

$$\hat{\mathcal{H}}_{\text{SW}} = E_{\text{GS}} + \sum_k \Omega_k \hat{\alpha}_k^\dagger \hat{\alpha}_k. \quad (\text{S.6})$$

This requires finding the eigenvalues and eigenvectors of a matrix containing the ω_{ij} and μ_{ij} coefficients. The squeezed ground state satisfies $\hat{\alpha}_k |\text{GS}\rangle = 0$, and is consequently an eigenstate of $\hat{\mathcal{H}}_{\text{SW}}$ with energy $E_{\text{GS}} < E_0 = \text{osc} \langle 0 | \hat{\mathcal{H}}_{\text{SW}} | 0 \rangle_{\text{osc}}$.

The correlations between the sites are contained in the covariance matrix of the coordinates and momenta,

$$\gamma_{IJ} = \frac{1}{2} \langle \text{GS} | \{ \hat{\zeta}_I, \hat{\zeta}_J^\dagger \} | \text{GS} \rangle, \quad (\text{S.7})$$

where $\hat{\zeta}_I = \hat{q}_i$ for $1 \leq I = i \leq N$ and $\hat{\zeta}_I = \hat{p}_i$ for $N+1 \leq I = i+N \leq 2N$. The covariance matrix completely characterizes the ground state, because the ground state of coupled harmonic oscillators is always a so-called Gaussian state [4]. In the $\hat{\alpha}_I$ operators diagonalizing the spin-wave Hamiltonian with $\hat{\alpha}_I = \hat{\alpha}_i$ for $1 \leq I = i \leq N$ and $\hat{\alpha}_I = \hat{\alpha}_i^\dagger$ for $N+1 \leq I = i+N \leq 2N$, the covariance matrix may be simply expressed as

$$\begin{aligned} \gamma_{IJ}^\alpha &= \frac{1}{2} \langle \text{GS} | \hat{\alpha}_I \hat{\alpha}_J^\dagger | \text{GS} \rangle - \frac{1}{2} \langle \text{GS} | [\hat{\alpha}_I, \hat{\alpha}_J^\dagger] | \text{GS} \rangle \\ &= \frac{1}{2} \delta_{IJ} \mathbb{1}(I \leq N) + \frac{1}{2} (-1)^{\mathbb{1}(I > N)} \delta_{IJ} \\ &= \frac{1}{2} \delta_{IJ} \mathbb{1}(I \leq N) + \frac{1}{2} \Sigma_{IJ}, \end{aligned} \quad (\text{S.8})$$

where $\mathbb{1}$ is the indicator function. This may be transformed to γ^a , the covariance matrix of the \hat{a}_I bosonic operators, using the transformation matrix

$$\mathcal{U}^{-1} = \begin{bmatrix} V & W \\ W^* & V^* \end{bmatrix} \quad (\text{S.9})$$

from Eq. (S.5). Since the transformation must preserve the bosonic commutation relations, i.e., $\mathcal{U} \Sigma \mathcal{U}^\dagger = \Sigma$ with

Σ from Eq. (S.8), \mathcal{U}^{-1} is a symplectic matrix which can be expressed using two $N \times N$ matrices V and W as given in Eq. (S.9). These matrices further satisfy the conditions

$$VV^\dagger - WW^\dagger = I, \quad (\text{S.10})$$

$$VW^T - WV^T = 0, \quad (\text{S.11})$$

$$V^\dagger V - (W^\dagger W)^* = I, \quad (\text{S.12})$$

$$V^\dagger W - W^T V^* = 0. \quad (\text{S.13})$$

Applying the transformations Eq. (S.5), then Eqs. (S.1) and (S.2) to Eq. (S.8), and using the conditions above, the covariance matrix in the canonical coordinates may be expressed as

$$\gamma = \frac{1}{2} \begin{bmatrix} (V^\dagger - W^\dagger)(V - W) & i[(V^\dagger - W^\dagger)(V + W) - I] \\ -i[(V^\dagger + W^\dagger)(V - W) - I] & (V^\dagger + W^\dagger)(V + W) \end{bmatrix} \quad (\text{S.14})$$

The covariance matrix γ describes the correlations between transversal spin components at certain lattice sites, and as such should be more readily accessible to local measurements than the eigenmodes α typically corresponding to extended states. However, there is a $U(1)$ gauge freedom in the definition of the covariance matrix, since the $e_{i,1}$ and $e_{i,2}$ directions used to define \hat{q}_i and \hat{p}_i in Eqs. (S.1) and (S.2) can be freely rotated around the classical equilibrium spin direction $\mathbf{S}_i^{(0)} = e_{i,3}$ while keeping the vectors orthonormal. It is useful to introduce the gauge-invariant symplectic eigenvalues of the covariance matrix, by using the eigenvalues $\pm ic_i$ of the matrix $-i\sigma^y \gamma$, where the $\sigma^y = \begin{bmatrix} 0 & -i \\ i & 0 \end{bmatrix}$ Pauli matrix acts on the subspace of coordinates and momenta. The symplectic eigenvalues may be used to define gauge-invariant correlation measures, of which we consider the relative information based on the von Neumann entropy and the logarithmic negativity in the main text. The symplectic nature of the transformation \mathcal{U}^{-1} ensures that the c_i are all non-negative real numbers.

The von Neumann entropy of the state with covariance matrix γ may be calculated from the symplectic eigenvalues as [5]

$$S_V(\gamma) = \sum_{i=1}^N f(2c_i), \quad (\text{S.15})$$

with

$$f(x) = \frac{x+1}{2} \ln\left(\frac{x+1}{2}\right) - \frac{x-1}{2} \ln\left(\frac{x-1}{2}\right). \quad (\text{S.16})$$

The relative information in a bipartite system based on the von Neumann entropy is defined as

$$S_{V,\text{rel}} = S_V(\gamma_1) + S_V(\gamma_2) - S_V(\gamma), \quad (\text{S.17})$$

where γ_1 and γ_2 are the covariance matrices of the two subsystems. These are simply submatrices of the

covariance matrix of the complete system, $\gamma_{1/2,II} = \{\gamma_{IJ}|I, J \in \mathcal{I}_{1/2}\}$, where the index sets $\mathcal{I}_{1/2}$ contain the degrees of freedom included in the first or the second subsystem. These expressions are equivalent for Gaussian states to the common definitions of the von Neumann entropy and relative information based on the density matrix and its partial traces, but the latter are more complicated to calculate in the infinite-dimensional Hilbert spaces considered here. The von Neumann entropy remains subadditive, which means that the relative information is non-negative. For a pure state, all of the symplectic eigenvalues are $c_i = 1/2$, and the von Neumann entropy vanishes. Therefore, the relative information may be used as a correlation measure, which for the two subsystems of a pure state measures purely quantum correlations or entanglement. If γ describes a mixed state, then $c_i \geq 1/2$ holds, and the relative information also contains classical correlations.

The logarithmic negativity is more useful for separating quantum and classical correlations from each other in mixed states. An important result in identifying separable or unentangled mixed states is the Peres-Horodecki criterion [6, 7]. For a given bipartition into subsystems 1 and 2, the partial transpose $\varrho_{(i_1 i_2), (j_1 j_2)}^{T_1} = \varrho_{(j_1 i_2), (i_1 j_2)}$ of the density matrix being also a density matrix, namely a positive semidefinite matrix which preserves the trace of 1 of the original density matrix, is a necessary condition for separability. While no sufficient condition for separability exists in the general case, the positivity of the partial transpose of the density matrix has been proven to be a sufficient condition in certain cases. For Gaussian states, these include all bipartitions where one of the subsystems consists of a single harmonic oscillator [8], satisfied by all pairs and clusters in the main text. On the level of the covariance matrix, partial transposition corresponds to reversing the sign of the momenta \hat{p}_i in one of the subsystems in Eq. (S.7). Using the symplectic eigenvalues \tilde{c}_i of the covariance matrix of the partial transposed system $\tilde{\gamma}$, the logarithmic negativity [9] may be defined as

$$E_{\mathcal{N}} = \sum_i \max\{0, -\log_2(2\tilde{c}_i)\}. \quad (\text{S.18})$$

The logarithmic negativity will be positive if $\tilde{c}_i < 1/2$ holds for any of the symplectic eigenvalues, which implies that the partial transpose of the density matrix is not positive (since $\tilde{c}_i \geq 1/2$ holds for density matrices), meaning that the state is not separable for the bipartitions mentioned above. In summary, when any subsystem is separated into a single harmonic oscillator and its environment, the logarithmic negativity will only be positive for entangled states, and its magnitude may be used as a measure of the quantum correlations in the system.

S.II. APPLICATION TO CONICAL SPIN SPIRALS

The covariance matrix γ in Eq. (S.7) may be calculated analytically for the spin spirals considered here. Following Ref. [10], we consider a more general Hamiltonian than in Eq. (1) in the main text,

$$\hat{\mathcal{H}} = \frac{1}{2} \sum_{i,j} J_{ij} \hat{\mathbf{S}}_i \cdot \hat{\mathbf{S}}_j + \frac{1}{2} \sum_{i,j} \mathbf{D}_{ij} (\hat{\mathbf{S}}_i \times \hat{\mathbf{S}}_j) - \mu_B g B_n \sum_i \mathbf{n} \cdot \hat{\mathbf{S}}_i \quad (\text{S.19})$$

where the J_{ij} are the Heisenberg interactions with no restriction to nearest- and next-nearest neighbors, \mathbf{D}_{ij} is the Dzyaloshinsky–Moriya vector [11, 12] between sites i and j , B_n is the projection of the external magnetic field on the direction \mathbf{n} , μ_B is the Bohr magneton and g is the gyromagnetic factor. The rotational plane of the spirals is determined solely by the Dzyaloshinsky–Moriya interactions, and the external field is applied perpendicular to the rotational plane to form a harmonic conical spin spiral [10].

We fix the gauge in the calculations by selecting the orthonormal basis used in Eqs. (S.1)-(S.3) as

$$\mathbf{e}_{i,1} = \begin{bmatrix} \sin(\mathbf{q}_0 \mathbf{R}_i) \cos \vartheta \\ \cos(\mathbf{q}_0 \mathbf{R}_i) \cos \vartheta \\ \sin \vartheta \end{bmatrix}, \quad (\text{S.20})$$

$$\mathbf{e}_{i,2} = \begin{bmatrix} -\cos(\mathbf{q}_0 \mathbf{R}_i) \\ \sin(\mathbf{q}_0 \mathbf{R}_i) \\ 0 \end{bmatrix}, \quad (\text{S.21})$$

$$\mathbf{e}_{i,3} = \begin{bmatrix} \sin(\mathbf{q}_0 \mathbf{R}_i) \sin \vartheta \\ \cos(\mathbf{q}_0 \mathbf{R}_i) \sin \vartheta \\ \cos \vartheta \end{bmatrix}, \quad (\text{S.22})$$

with the components expressed in a global right-handed basis $\{\mathbf{e}_1, \mathbf{e}_2, \mathbf{n}\}$.

After performing the Holstein–Primakoff transformation in Eqs. (S.1)-(S.3), the spin-wave Hamiltonian may be written in a simple form following Fourier transformation of the bosonic operators,

$$\hat{a}_{\mathbf{q}} = \frac{1}{\sqrt{N}} \sum_i e^{-i\mathbf{q} \cdot \mathbf{R}_i} \hat{a}_i, \quad (\text{S.23})$$

$$\hat{a}_{\mathbf{q}}^\dagger = \frac{1}{\sqrt{N}} \sum_i e^{i\mathbf{q} \cdot \mathbf{R}_i} \hat{a}_i^\dagger, \quad (\text{S.24})$$

and of the interaction coefficients,

$$J_{\mathbf{q}} = \sum_{\mathbf{R}_i - \mathbf{R}_j} e^{-i\mathbf{q} \cdot (\mathbf{R}_i - \mathbf{R}_j)} J_{ij}, \quad (\text{S.25})$$

$$D_{\mathbf{q}}^n = \sum_{\mathbf{R}_i - \mathbf{R}_j} e^{-i\mathbf{q} \cdot (\mathbf{R}_i - \mathbf{R}_j)} \mathbf{D}_{ij} \cdot \mathbf{n}, \quad (\text{S.26})$$

$$\tilde{J}_{\mathbf{q}} = J_{\mathbf{q}} + iD_{\mathbf{q}}^n. \quad (\text{S.27})$$

Introducing the coefficients

$$D_0(\mathbf{q}) = S \left(1 - \frac{\sin^2 \vartheta}{2} \right) \frac{1}{2} (\tilde{J}_{\mathbf{q}_0+\mathbf{q}} + \tilde{J}_{\mathbf{q}_0-\mathbf{q}}) + S \frac{\sin^2 \vartheta}{2} \frac{1}{2} (\tilde{J}_{\mathbf{q}} + \tilde{J}_{-\mathbf{q}}) - S \tilde{J}_{\mathbf{q}_0}, \quad (\text{S.28})$$

$$D_{\text{nr}}(\mathbf{q}) = S \cos \vartheta \frac{1}{2} (\tilde{J}_{\mathbf{q}_0+\mathbf{q}} - \tilde{J}_{\mathbf{q}_0-\mathbf{q}}), \quad (\text{S.29})$$

$$D_a(\mathbf{q}) = -S \frac{\sin^2 \vartheta}{2} \frac{1}{2} (\tilde{J}_{\mathbf{q}_0+\mathbf{q}} + \tilde{J}_{\mathbf{q}_0-\mathbf{q}}) + S \frac{\sin^2 \vartheta}{2} \frac{1}{2} (\tilde{J}_{\mathbf{q}} + \tilde{J}_{-\mathbf{q}}), \quad (\text{S.30})$$

the spin-wave Hamiltonian in Eq. (S.4) may be rewritten in a block-diagonal form of 2×2 blocks,

$$\hat{\mathcal{H}}_{\text{SW}} = \tilde{E}_0 + \frac{1}{2} \sum_{\mathbf{q}} \left[(D_0(\mathbf{q}) + D_{\text{nr}}(\mathbf{q})) \hat{a}_{\mathbf{q}}^\dagger \hat{a}_{\mathbf{q}} + D_a(\mathbf{q}) \hat{a}_{\mathbf{q}}^\dagger \hat{a}_{-\mathbf{q}}^\dagger + D_a(\mathbf{q}) \hat{a}_{-\mathbf{q}} \hat{a}_{\mathbf{q}} + (D_0(\mathbf{q}) - D_{\text{nr}}(\mathbf{q})) \hat{a}_{-\mathbf{q}} \hat{a}_{-\mathbf{q}}^\dagger \right]. \quad (\text{S.31})$$

Note that all coefficients are real in this gauge, and the relations $D_0(\mathbf{q}) = D_0(-\mathbf{q})$, $D_{\text{nr}}(\mathbf{q}) = -D_{\text{nr}}(-\mathbf{q})$, and $D_a(\mathbf{q}) = D_a(-\mathbf{q})$ hold. The influence of the magnetic field is included in the ϑ parameter related to the opening angle of the spiral cone, $\cos \vartheta = \mu_B g B_n / (S \tilde{J}_0 - S \tilde{J}_{\mathbf{q}})$. Thus, the operators belonging to the eigenmodes of the system may be written as

$$\hat{\alpha}_{\mathbf{q}} = v_{\mathbf{q}} \hat{a}_{\mathbf{q}} + w_{\mathbf{q}} \hat{a}_{-\mathbf{q}}^\dagger, \quad (\text{S.32})$$

with the coefficients

$$v_{\mathbf{q}} = \sqrt{\frac{1}{2} \left(\frac{D_0(\mathbf{q})}{\sqrt{D_0^2(\mathbf{q}) - D_a^2(\mathbf{q})}} + 1 \right)}, \quad (\text{S.33})$$

$$w_{\mathbf{q}} = \sqrt{\frac{1}{2} \left(\frac{D_0(\mathbf{q})}{\sqrt{D_0^2(\mathbf{q}) - D_a^2(\mathbf{q})}} - 1 \right)}. \quad (\text{S.34})$$

Note that the matrices introduced in Eq. (S.9) are diagonal in Fourier space, $V_{\mathbf{q}\mathbf{q}'} = v_{\mathbf{q}} \delta_{\mathbf{q}\mathbf{q}'}$ and $W_{\mathbf{q}\mathbf{q}'} = w_{\mathbf{q}} \delta_{\mathbf{q}\mathbf{q}'}$, the elements are symmetric under switching the sign of \mathbf{q} , and are chosen to be real valued. They are normalized according to the relations in Eq. (S.10)-(S.13). Performing inverse Fourier transformation and using Eq. (S.14), the covariance matrix may be written in the compact form of

$$\gamma_{ij} = \begin{bmatrix} \gamma_{i,j} & \gamma_{i,j+N} \\ \gamma_{i+N,j} & \gamma_{i+N,j+N} \end{bmatrix} = \frac{1}{2N} \sum_{\mathbf{q}} \begin{bmatrix} \sqrt{\frac{D_0(\mathbf{q}) - D_a(\mathbf{q})}{D_0(\mathbf{q}) + D_a(\mathbf{q})}} & 0 \\ 0 & \sqrt{\frac{D_0(\mathbf{q}) + D_a(\mathbf{q})}{D_0(\mathbf{q}) - D_a(\mathbf{q})}} \end{bmatrix} \cos[\mathbf{q} \cdot (\mathbf{R}_i - \mathbf{R}_j)]. \quad (\text{S.35})$$

Note that the covariance matrix only depends on the relative position of the two sites, which is a consequence of

Fourier transformation being suitable for diagonalizing the spin-wave Hamiltonian. Furthermore, the covariance matrix is independent of the spin quantum number S , as can be seen after expressing the coefficients in the matrix using Eqs. (S.28) and (S.30),

$$D_0(\mathbf{q}) - D_a(\mathbf{q}) = S \frac{1}{2} (\tilde{J}_{\mathbf{q}_0+\mathbf{q}} + \tilde{J}_{\mathbf{q}_0-\mathbf{q}}) - S \tilde{J}_{\mathbf{q}_0}, \quad (\text{S.36})$$

$$\begin{aligned} D_0(\mathbf{q}) + D_a(\mathbf{q}) &= S (1 - \sin^2 \vartheta) \frac{1}{2} (\tilde{J}_{\mathbf{q}_0+\mathbf{q}} + \tilde{J}_{\mathbf{q}_0-\mathbf{q}}) \\ &\quad + S \sin^2 \vartheta \frac{1}{2} (\tilde{J}_{\mathbf{q}} + \tilde{J}_{-\mathbf{q}}) - S \tilde{J}_{\mathbf{q}_0}, \end{aligned} \quad (\text{S.37})$$

and taking their ratio. Since \mathbf{q}_0 was found by minimizing $\tilde{J}_{\mathbf{q}}$ in order to obtain the ground state, clearly both $D_0(\mathbf{q}) - D_a(\mathbf{q})$ and $D_0(\mathbf{q}) + D_a(\mathbf{q})$ are non-negative. It can also be seen from the expressions that $D_0(\mathbf{q}) - D_a(\mathbf{q})$ vanishes for $\mathbf{q} = \mathbf{0}$. This is connected to a zero mode of the system, found by calculating the eigenfrequencies in Eq. (S.6),

$$\Omega_{\mathbf{q}} = D_{\text{nr}}(\mathbf{q}) + \sqrt{D_0^2(\mathbf{q}) - D_a^2(\mathbf{q})}. \quad (\text{S.38})$$

The eigenfrequency also vanishes for $\mathbf{q} = \mathbf{0}$ because of $D_{\text{nr}}(\mathbf{0}) = 0$. This mode describes the continuous translation of the spiral along the wave vector, or a change in the phase of the spiral, which costs no energy. This implies that the summation over the \mathbf{q} points in Eq. (S.35) must be performed carefully to avoid the singularity at $\mathbf{q} = \mathbf{0}$. For this purpose, the summation is performed numerically over a regular grid in \mathbf{q} space which does not include the $\mathbf{q} = \mathbf{0}$ point, similarly to the Monkhorst–Pack method [13, 14] but adapted to preserve a C_{3v} symmetry of the grid points around $\mathbf{q} = \mathbf{0}$ on the triangular lattice. Expanding the Fourier transforms of the interaction parameters yields $D_0(\mathbf{q}) - D_a(\mathbf{q}) \propto \mathbf{q}^2$ apart from specific coefficient values, which are typically found at the phase transitions. This means that the singularity $\sqrt{D_0(\mathbf{q}) + D_a(\mathbf{q})} / \sqrt{D_0(\mathbf{q}) - D_a(\mathbf{q})} \propto \mathbf{q}^{-1}$ is integrable in at least two dimensions, so the calculations should converge as the mesh is refined.

The elements of the covariance matrix in Fourier space,

$$\gamma_{\mathbf{q}}^{(1)} = \frac{1}{2} \sqrt{\frac{D_0(\mathbf{q}) - D_a(\mathbf{q})}{D_0(\mathbf{q}) + D_a(\mathbf{q})}}, \quad (\text{S.39})$$

$$\gamma_{\mathbf{q}}^{(2)} = \frac{1}{2} \sqrt{\frac{D_0(\mathbf{q}) + D_a(\mathbf{q})}{D_0(\mathbf{q}) - D_a(\mathbf{q})}}, \quad (\text{S.40})$$

are illustrated in Fig. S1 for different parameter sets. The zero mode at $\mathbf{q} = \mathbf{0}$ shows up as a singularity in $\gamma_{\mathbf{q}}^{(2)}$ in Fig. S1(b) and (d). If only isotropic exchange interactions are taken into account, and the spiral is planar ($\sin \vartheta = 1$), then $D_0(\mathbf{q}) + D_a(\mathbf{q})$ will vanish for $\mathbf{q} = \mathbf{q}_0$ and all symmetrically equivalent points satisfying $\tilde{J}_{\mathbf{q}_\alpha} = \tilde{J}_{\mathbf{q}_0}$. This can be explained by the system possessing another zero mode, namely that the rotational

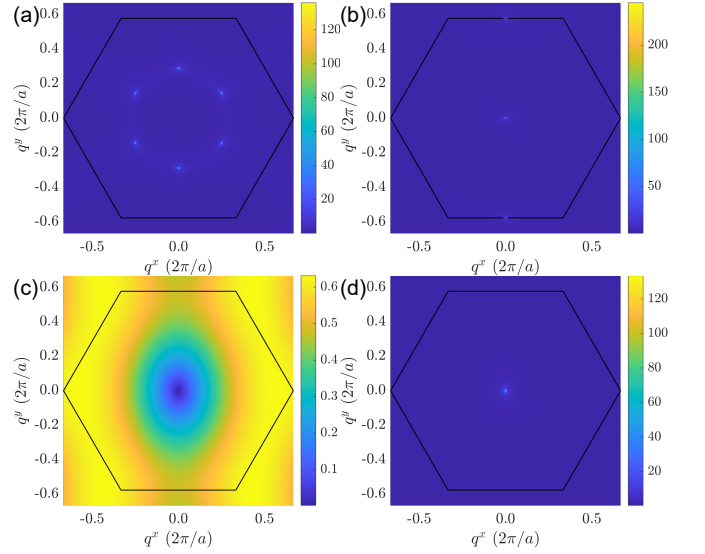


FIG. S1. Elements of the covariance matrix in Fourier space. (a) $\gamma_{\mathbf{q}}^{(1)}$ in Eq. (S.39) and (b) $\gamma_{\mathbf{q}}^{(2)}$ in Eq. (S.40) calculated for the parameters $J_2 = -J_1 > 0, D_1 = 0$. (c) $\gamma_{\mathbf{q}}^{(1)}$ and (d) $\gamma_{\mathbf{q}}^{(2)}$ calculated for the parameters $J_2 = J_1 = 0, D_1 > 0$. The black hexagon illustrates the Brillouin zone, consisting of an $N = 513 \times 513$ grid.

plane of the spiral may be chosen arbitrarily. This zero mode leads to singularities in $\gamma_{\mathbf{q}}^{(1)}$, as shown in Fig. S1(a). This zero mode is lifted if an external magnetic field is applied or the Dzyaloshinsky–Moriya interaction is taken into account, as illustrated by the much narrower range of values in the colorbar in Fig. S1(c).

The two-mode squeezing parameters $r_{\mathbf{q}}$ connecting the eigenmodes with \mathbf{q} and $-\mathbf{q}$ derived in Ref. [10] are connected to the elements of the covariance matrix in Eqs. (S.39) and (S.40), namely

$$e^{2r_{\mathbf{q}}} = \sqrt{\frac{D_0(\mathbf{q}) + |D_a(\mathbf{q})|}{D_0(\mathbf{q}) - |D_a(\mathbf{q})|}} = 2 \max \left\{ \gamma_{\mathbf{q}}^{(1)}, \gamma_{\mathbf{q}}^{(2)} \right\}. \quad (\text{S.41})$$

Due to the simple structure of the covariance matrix, the symplectic eigenvalues for one and two lattice sites may also be expressed in a compact form,

$$c_i = \sqrt{\gamma_{i,i} \gamma_{i+N,i+N}}, \quad (\text{S.42})$$

and

$$c_{ij}^{(1)} = \sqrt{(\gamma_{i,i} + \gamma_{i,j})(\gamma_{i+N,i+N} + \gamma_{i+N,j+N})}, \quad (\text{S.43})$$

$$c_{ij}^{(2)} = \sqrt{(\gamma_{i,i} - \gamma_{i,j})(\gamma_{i+N,i+N} - \gamma_{i+N,j+N})}, \quad (\text{S.44})$$

with the coefficients defined in Eq. (S.35). These expressions may be used to calculate the two-site relative information based on the von Neumann entropy in Eq. (S.17). The partial transposition required for the logarithmic

negativity in Eq. (S.18) corresponds to switching the sign of $\gamma_{i+N,j+N}$ in the two-site expression.

These analytic expressions make it possible to draw some qualitative conclusions on the distance dependence of the logarithmic negativity. Due to the singularity of $\gamma_{\mathbf{q}}^{(2)}$ at $\mathbf{q} = \mathbf{0}$, its Fourier transform at $\mathbf{R}_i - \mathbf{R}_j = \mathbf{0}$ $\gamma_{i+N,i+N}$ is typically considerably larger than $1/2$. The other on-site coefficient $\gamma_{i,i}$ is also quite large if there are singularities in $\gamma_{\mathbf{q}}^{(1)}$ (see Fig. S1(a)), but it is close to $1/2$ if $\gamma_{\mathbf{q}}^{(1)}$ is smooth (see Fig. S1(c)), because it would take the value $\gamma_{i,i} = 1/2$ in the uncorrelated case where $\gamma_{\mathbf{q}}^{(1)} \equiv 1/2$. Since the correlation matrix elements decrease rapidly with the distance between i and j , at large distances one obtains $\tilde{c}_{ij}^{(1)} \approx \tilde{c}_{ij}^{(2)} \approx c_i > 1/2$, and the logarithmic negativity between the two sites in Eq. (S.18) vanishes. Because both $\gamma_{i,i}$ and $\gamma_{i+N,i+N}$ are large in the isotropic model with nearest- and next-nearest-neighbor Heisenberg interactions J_1 and J_2 , the logarithmic negativity vanishes for all pairs for certain parameter ranges. However, this is not observed for any parameter set if only nearest-neighbor Heisenberg and Dzyaloshinsky–Moriya interactions J_1 and D_1 are considered, where $\gamma_{\mathbf{q}}^{(1)}$ is not singular. This is illustrated in Fig. S2. In this model, the system transforms from the ferromagnetic state at $J_1 < 0, D_1 = 0$ to the Néel antiferromagnetic state $J_1 > 0, D_1 = 0$ through a spin spiral with ordering vector parallel to the x axis as the angle $\text{atan2}(D_1, J_1)$ is varied between $-\pi/2$ and $\pi/2$. The wave vector depends almost linearly on the angle, particularly close to the ferromagnetic state. The sum of the pairwise logarithmic negativity is finite everywhere, apart from the abrupt drop to zero in the ferromagnetic state; in particular, the logarithmic negativity between nearest-neighbor pairs also remains finite. The logarithmic negativity calculated with the 12-site environment also used in Fig. 2 is even smoother and closely follows the monotonic change in q_0 with $\text{atan2}(D_1, J_1)$.

Due to the singularity of $\gamma_{\mathbf{q}}^{(1)}$ at the points \mathbf{q}_{α} symmetric equivalent to \mathbf{q}_0 , the covariance matrix elements in Eq. (S.35) may be approximated as

$$\gamma_{i,j} \approx \sum_{\alpha} f(|\mathbf{R}_i - \mathbf{R}_j|) \cos[\mathbf{q}_{\alpha} \cdot (\mathbf{R}_i - \mathbf{R}_j)] \quad (\text{S.45})$$

by performing the summation around the singularities which give the largest contribution to the sum. Here, the $f(|\mathbf{R}_i - \mathbf{R}_j|)$ function shows a similar power-law decay with negligible oscillations around each singularity \mathbf{q}_{α} , while the $\cos[\mathbf{q}_{\alpha} \cdot (\mathbf{R}_i - \mathbf{R}_j)]$ causes oscillations with the distance with the characteristic wave vectors of the spiral \mathbf{q}_{α} . As illustrated in Fig. 4(b) in the main text, these oscillations become observable in the logarithmic negativity calculated for increasing environments. However, these oscillations are absent in Fig. S3 for the

same quantity calculated in spin spirals stabilized by the Dzyaloshinsky–Moriya interaction D_1 instead of J_2 , where the zero mode connected to the rotational plane of the spiral and the accompanying singularities in the

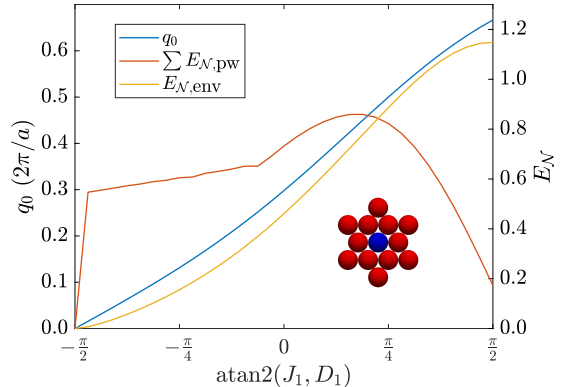


FIG. S2. Phase diagram and logarithmic negativity for the Dzyaloshinsky–Moriya-interaction-driven spin spirals. Ordering wave vector of the spiral q_0 , pairwise logarithmic negativity $\sum E_{N,pw}$ summed up over all sites, and logarithmic negativity $E_{N,env}$ with the environment as a function of the ratio of nearest-neighbor and next-nearest-neighbor exchange couplings. The center site (blue) and the environment containing all nearest- and next-nearest-neighbour sites (red) used as a bipartition for calculating $E_{N,env}$ is sketched. The Brillouin zone integration was performed on an $N = 513 \times 513$ grid.

correlations are absent. The fitting parameters to the asymptotics of these correlation functions are given in Sec. S.III.

S.III. ASYMPTOTICS OF THE CORRELATION FUNCTIONS

The parameters of the functions fitted to the correlation functions $dE_{N,env}/dy$ and $dE_{N,env}/dx$ in Figs. 4(a), 4(b), and S3 are collected in Tables I, II, and III, respectively. In the row-wise antiferromagnetic state of the frustrated Heisenberg model, $dE_{N,env}/dy$ is well described by a power law in Table I, with the absolute value of the exponent η decreasing as the phase transition to the Néel antiferromagnetic state is approached. In the spin-spiral state, the power law is modulated by a harmonic function with wave number k , which agrees well with the wave number of the spiral q_0 as shown in Table II. The errors of the fit for the exponent are too large to establish a clear trend in this regime. In the Dzyaloshinsky–Moriya-interaction-driven spin spirals, the oscillations are absent in $dE_{N,env}/dx$, and the absolute value of the exponent of the power law appears to increase as the ferromagnetic state is approached.

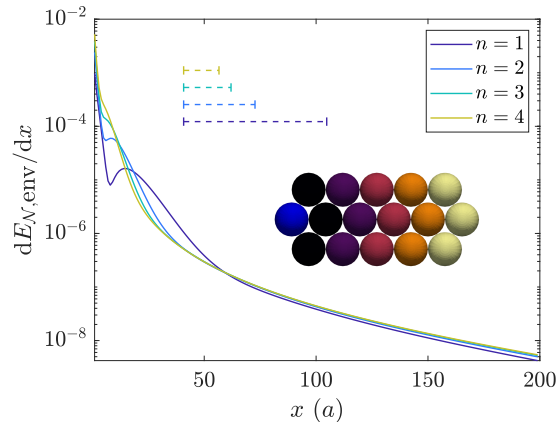


FIG. S3. Derivative of the logarithmic negativity with the environment along the modulation direction for the Dzyaloshinsky–Moriya-interaction-driven spin spirals close to the transition from the spin-spiral state to the ferromagnetic state ($\text{atan2}(J_1, D_1) = -\pi/2 + n\pi/2^5$). The logarithmic negativity was calculated for the bipartition on the leftmost site (blue) and the environment (yellow to purple atoms). In each step, the environment was increased by three atoms denoted by the same color. $dE_{N,\text{env}}/dx$ is the logarithmic negativity differentiated with respect to the size of the environment. Dashed lines illustrate the spin-spiral period p for the given parameters. The Brillouin zone integration was performed on an $N = 1026 \times 1026$ grid.

n	η
1	2.54 ± 0.04
2	2.60 ± 0.05
3	2.64 ± 0.05
4	2.69 ± 0.05
5	2.73 ± 0.05

TABLE I. Exponents of the correlation function in the frustrated Heisenberg model in the row-wise antiferromagnetic state shown in Fig. 4(a) in the main text. The fitted function was $dE_{N,\text{env}}/dy = ay^{-\eta}$. The interaction parameters are $\text{atan2}(J_2, J_1) = 5\pi/2^7 + n\pi/2^8$.

n	η	k ($2\pi/a$)	q_0 ($2\pi/a$)
1	2.27 ± 0.13	0.0683 ± 0.0004	0.0682
2	2.14 ± 0.14	0.0521 ± 0.0005	0.0517
3	2.16 ± 0.12	0.0260 ± 0.0004	0.0254

TABLE II. Fitting parameters of the correlation function in the Dzyaloshinsky–Moriya model in the spin-spiral state shown in Fig. 4(b) in the main text. The fitted function was $dE_{N,\text{env}}/dy = [a + b \cos(ky + \varphi)]y^{-\eta}$. The interaction parameters are $\text{atan2}(J_2, J_1) = 1829\pi/2^{11} + n\pi/2^9$. The wave number of the spiral q_0 is given for comparison with the modulation parameter k .

n	η
1	2.93 ± 0.02
2	2.88 ± 0.01
3	2.85 ± 0.01
4	2.82 ± 0.01

TABLE III. Exponents of the correlation functions in the Dzyaloshinsky–Moriya model in the spin-spiral state shown in Fig. S3. The fitted function was $dE_{\mathcal{N},\text{env}}/dx = ax^{-\eta}$. The interaction parameters are $\text{atan2}(J_1, D_1) = -\pi/2 + n\pi/2^5$.

-
- [1] L. D. Landau and E. M. Lifshitz, *Phys. Z. Sowjetunion* **8**, 153 (1935).
- [2] T. L. Gilbert, *IEEE Trans. Magn.* **40**, 3443 (2004).
- [3] T. Holstein and H. Primakoff, *Phys. Rev.* **58**, 1098 (1940).
- [4] J. Eisert and M. B. Plenio, *International Journal of Quantum Information* **01**, 479–506 (2003).
- [5] G. Adesso and F. Illuminati, *Journal of Physics A: Mathematical and Theoretical* **40**, 7821–7880 (2007).
- [6] A. Peres, *Phys. Rev. Lett.* **77**, 1413 (1996).
- [7] M. Horodecki, P. Horodecki, and R. Horodecki, *Physics Letters A* **223**, 1–8 (1996).
- [8] R. Simon, *Phys. Rev. Lett.* **84**, 2726 (2000).
- [9] G. Vidal and R. F. Werner, *Phys. Rev. A* **65**, 032314 (2002).
- [10] D. Wuhler, L. Rózsa, U. Nowak, and W. Belzig, *Phys. Rev. Res.* **5**, 043124 (2023).
- [11] I. Dzyaloshinsky, *Journal of Physics and Chemistry of Solids* **4**, 241 (1958).
- [12] T. Moriya, *Phys. Rev.* **120**, 91 (1960).
- [13] H. J. Monkhorst and J. D. Pack, *Phys. Rev. B* **13**, 5188 (1976).
- [14] J. D. Pack and H. J. Monkhorst, *Phys. Rev. B* **16**, 1748 (1977).